Electronic Supplementary Information for:

Time-resolved spectra of I_2 in a krypton crystal by G-MCTDH simulations: Nonadiabatic dynamics, dissipation and environment driven decoherence

David Picconi and Irene Burghardt

Institute of Physical and Theoretical Chemistry, Goethe University Frankfurt
Max-von-Laue-Straße 7, D-60438 Frankfurt am Main, Germany
E-mail: picconi@chemie.uni-frankfurt.de

1 Diatomics-in-molecules construction of the potential energy surfaces of the I_2Kr_{72} cluster

1.1 Covalent states

As explained in the Appendix of the main paper, the valence spin-orbital basis for the I atoms is set in the coupled representation $|J_k M_k\rangle$ of the total angular momentum $\mathbf{J} = \mathbf{L} + \mathbf{S}$, where M_k is the eigenvalue of the component of $\mathbf{J}$ along the internuclear axis. Since each ^2P atom has six valence orbitals ($J = \frac{1}{2}, \frac{3}{2}$, with $M = -J, ..., J$), 36 molecular diabatic states can be constructed, whose wavefunctions have the asymptotic form

$$|\psi_j\rangle = \sum_{k=1}^{36} C_{jk} \left| J_k^{(A)} M_k^{(A)} \right\rangle \left| J_k^{(B)} M_k^{(B)} \right\rangle \ , \tag{S1}$$

where the superscripts (A) and (B) refer to the two I atoms.

The 36×36 diabatic potential matrix consists of different contributions accounting for all atom-atom pairwise interactions,

$$\mathbf{V} = \mathbf{V}_{\mathrm{I}_A\mathrm{I}_B} + \sum_{i=1}^{N_{\mathrm{Kr}}} \mathbf{V}_{\mathrm{I}_A\mathrm{Kr}_i} + \sum_{i=1}^{N_{\mathrm{Kr}}} \mathbf{V}_{\mathrm{I}_B\mathrm{Kr}_i} + \sum_{i=1}^{N_{\mathrm{Kr}}-1} \sum_{j=i+1}^{N_{\mathrm{Kr}}} \mathbf{V}_{\mathrm{Kr}_i\mathrm{Kr}_j} \ , \tag{S2}$$

where N_{Kr} is the number of Kr atoms included in the model. The I–I interaction matrix $\mathbf{V}_{\mathrm{I}_A\mathrm{I}_B}$ is diagonal, in agreement with the observation that the coupling between different electronic states is primarily induced by the environment.[1,2] In our implementation, we used the 36 diagonal potential energy curves calculated by Teichteil and Pelissier at the coupled cluster level,[3] including relativistic contributions. The potential matrices $\mathbf{V}_{\mathrm{Kr}_i\mathrm{Kr}_j}$ are multiples of the identity and the $\mathrm{Kr} - \mathrm{Kr}$ interactions were modelled using the Buckingham-type function of Ref. 4 .

The couplings between the different diabatic states are induced by the interactions between the Kr matrix and the two iodine atoms, I_A and I_B, represented by the matrices $\mathbf{V}_{\mathrm{I}_A\mathrm{Kr}_i}$ and $\mathbf{V}_{\mathrm{I}_B\mathrm{Kr}_i}$

of Eq. (S2). These matrices are first expressed in the $\left\{\left|J_k^{(A)}M_k^{(A)}\right\rangle\left|J_k^{(B)}M_k^{(B)}\right\rangle\right\}$ basis as Kronecker products and then transformed to the symmetry adapted basis as

$$\mathbf{V}_{\mathrm{I}_A\mathrm{Kr}_i} = \mathbf{C}^\dagger \mathbf{V}_{\mathrm{IKr}}(R_{Ai},\Omega_{Ai}) \otimes \mathbf{I}_{6\times 6}\mathbf{C} \quad \text{and} \quad \mathbf{V}_{\mathrm{I}_B\mathrm{Kr}_i} = \mathbf{C}^\dagger \mathbf{I}_{6\times 6} \otimes \mathbf{V}_{\mathrm{IKr}}(R_{Bi},\Omega_{Bi})\mathbf{C}\,, \tag{S3}$$

where $\mathbf{I}_{6\times 6}$ is the 6×6 identity matrix and the $\mathbf{C}$ matrix contains the coefficients of Eq. (S1), given explicitly in the Appendix of the main paper (see Table 1). $R_{\alpha i}$ is the $\mathrm{I}_\alpha - \mathrm{Kr}_i$ distance ($\alpha = A,B$) and $\Omega_{\alpha i}$ is a set of Euler angles which define the relative orientation between two reference frames: (i) An "interaction" frame ($x'y'z'$) where the z' axis is aligned to the direction of the $\mathrm{I}_\alpha - \mathrm{Kr}_i$ bond, and (ii) the body-fixed frame (xyz) anchored to the chromophore, oriented such that the z axis is aligned to the I–I bond and the x axis lies in the $x''z''$ plane of the space-fixed frame, defined by the frozen Kr cage. The basis set and the resulting diabatic Hamiltonian refer to the body-fixed system, whereas the different 6×6 I–Kr interaction matrices $\mathbf{V}_{\mathrm{IKr}}(R,0)$ are conveniently calculated in the $x'y'z'$ frames of the respective atom pairs, where they take the standard form[5,6] given in Table S1. The transformations to the common xyz system are performed using Wigner rotation matrices,

$$\mathbf{V}_{\mathrm{IKr}}(R,\Omega) = \left[\mathbf{D}^{\frac{1}{2}}(\Omega)\oplus\mathbf{D}^{\frac{3}{2}}(\Omega)\right]^\dagger \mathbf{V}_{\mathrm{IKr}}(R,0)\left[\mathbf{D}^{\frac{1}{2}}(\Omega)\oplus\mathbf{D}^{\frac{3}{2}}(\Omega)\right]\,. \tag{S4}$$

The distance-dependent potentials V_Σ and V_Π, which define the matrix $\mathbf{V}_{\mathrm{IKr}}(R,0)$ have been modelled using Morse-Morse-switching function-van der Waals potentials derived from zero electron kinetic energy (ZEKE) spectroscopic measurements.[7]

Table S1 The 6×6 I–Kr interaction matrix $\mathbf{V}_{\mathrm{IKr}}(R,0)$ in the interaction frame, where $|J,M\rangle$ basis refer to the I–Kr connecting axis [see Eq. (S4)]

$\lvert J,M\rangle$	$\left\lvert\frac{1}{2},\pm\frac{1}{2}\right\rangle$	$\left\lvert\frac{3}{2},\pm\frac{3}{2}\right\rangle$	$\left\lvert\frac{3}{2},\pm\frac{1}{2}\right\rangle$
$\left\lvert\frac{1}{2},\pm\frac{1}{2}\right\rangle$	$\delta_{MM'}\left(V_\Sigma+2V_\Pi\right)/3$	0	$\pm\delta_{MM'}\sqrt{2}\left(V_\Pi-V_\Sigma\right)/3$
$\left\lvert\frac{3}{2},\pm\frac{3}{2}\right\rangle$	0	$\delta_{MM'}V_\Pi$	0
$\left\lvert\frac{3}{2},\pm\frac{1}{2}\right\rangle$	$\pm\delta_{MM'}\sqrt{2}\left(V_\Pi-V_\Sigma\right)/3$	0	$\delta_{MM'}\left(2V_\Sigma+V_\Pi\right)/3$

1.2 Ion pair manifold

As explained in the Appendix of the main paper, the diabatic states of the ion pair manifold are represented by structures in which the Kr atoms are in their ground state, the I^- anion has an S closed shell and the I^+ cation has a ^3P structure, associated to nine $|J_kM_k\rangle$ terms ($J_k = 0,1,2$). Accounting for both $\mathrm{I}^-\mathrm{I}^+$ and $\mathrm{I}^+\mathrm{I}^-$ configurations yields a total of 18 diabatic states of the form

$$|\overline{\Psi}_j\rangle = \sum_{k=1}^{9}\overline{C}_{jk}\left|J_k^{(A)}M_k^{(A)}\right\rangle\left|S^{(B)}\right\rangle + \sum_{k=10}^{18}\overline{C}_{jk}\left|S^{(A)}\right\rangle\left|J_k^{(B)}M_k^{(B)}\right\rangle\,. \tag{S5}$$

Similarly to the covalent manifold, the coefficients $\overline{C}_{jk}$ form a 18×18 matrix and are defined in order to obtain electronic states belonging to one of the irreps of the $D_{2\mathrm{h}}$ point group. The explicit form of the states of Eq. (S5) is given in Ref. 8. The 18 ion pair levels are energetically separated into two tiers, and only transitions to the lowest tier are considered in this work. The

relevant states, associated with ten $^3P_2$ structures, are reported in Table 2 of the Appendix of the main paper, and their irrep is indicated.

The diabatic 18×18 ion pair potential matrix is a sum of different atom-atom interaction terms,

$$\mathbf{W} = \mathbf{W}_{\mathrm{I}_A\mathrm{I}_B} + \sum_{i=1}^{N_{\mathrm{Kr}}} \mathbf{W}_{\mathrm{I}_A\mathrm{Kr}_i} + \sum_{i=1}^{N_{\mathrm{Kr}}} \mathbf{W}_{\mathrm{I}_B\mathrm{Kr}_i} + \sum_{i=1}^{N_{\mathrm{Kr}}-1} \sum_{j=i+1}^{N_{\mathrm{Kr}}} \mathbf{W}_{\mathrm{Kr}_i\mathrm{Kr}_j} + \mathbf{W}_{\mathrm{pol}} \ . \tag{S6}$$

Similarly to the covalent manifold, $\mathbf{W}_{\mathrm{I}_A\mathrm{I}_B}$ is the diagonal matrix which contains ion-pair potential energy curves derived from detailed analysis of the emission spectra[9] and modelled using the Morse potentials of Ref. 8. The matrices $\mathbf{W}_{\mathrm{Kr}_i\mathrm{Kr}_j}$ are multiple of the identity and defined by the same Kr–Kr interaction potential used for the covalent manifold.

The Kr environment induces the coupling between different diabatic states. The interactions between the Kr and the iodine atoms I_A and I_B are described by the matrices $\mathbf{W}_{\mathrm{I}_A\mathrm{Kr}_i}$ and $\mathbf{W}_{\mathrm{I}_B\mathrm{Kr}_i}$, respectively, which are evaluated in the basis $\left\{ \left| J_k^{(A)} M_k^{(A)} \right\rangle \left| S^{(B)} \right\rangle ; \left| S^{(A)} \right\rangle \left| J_k^{(B)} M_k^{(B)} \right\rangle \right\}$ and then transformed to the symmetry adapted basis as follows:

$$\mathbf{W}_{\mathrm{I}_A\mathrm{Kr}_i} = \mathbf{C}^\dagger \left[\mathbf{W}_{\mathrm{I}^+\mathrm{Kr}}(R_{Ai}, \Omega_{Ai}) \oplus \mathbf{I}_{9\times 9} W_{\mathrm{I}^-\mathrm{Kr}}(R_{Ai}) \right] \mathbf{C} \ , \tag{S7a}$$

$$\mathbf{W}_{\mathrm{I}_B\mathrm{Kr}_i} = \mathbf{C}^\dagger \left[\mathbf{I}_{9\times 9} W_{\mathrm{I}^-\mathrm{Kr}}(R_{Bi}) \oplus \mathbf{W}_{\mathrm{I}^+\mathrm{Kr}}(R_{Bi}, \Omega_{Bi}) \right] \mathbf{C} \ , \tag{S7b}$$

where $W_{\mathrm{I}^-\mathrm{Kr}}(R)$ is the pair potential between the iodine anion and the krypton anion, for which the expression derived from the experiments of Ref. 7 is used. The 9×9 matrix $\mathbf{W}_{\mathrm{I}^+\mathrm{Kr}}(R, \Omega)$ describes the interaction between the Kr atoms and the ^3P cation I^+. Similarly to the case of the ^2P atom discussed in Sect. 1.1, this matrix conveniently set up in the reference frame $x'y'z'$ where the z' axis is aligned to the I–Kr direction, and the potential matrix takes the form of Table S2.[10] The transformation to the body-fixed frame is performed using Wigner rotation matrices,

$$\mathbf{W}_{\mathrm{I}^+\mathrm{Kr}}(R, \Omega) = \left[\mathbf{D}^0(\Omega) \oplus \mathbf{D}^1(\Omega) \oplus \mathbf{D}^2(\Omega) \right]^\dagger \mathbf{W}_{\mathrm{I}^+\mathrm{Kr}}(R, 0) \left[\mathbf{D}^0(\Omega) \oplus \mathbf{D}^1(\Omega) \oplus \mathbf{D}^2(\Omega) \right] \ . \tag{S8}$$

The $\mathrm{I}^+ \cdots \mathrm{Kr}$ pair potentials $W_\Sigma(R)$ and $W_\Pi(R)$, defining the matrix $\mathbf{W}_{\mathrm{I}^+\mathrm{Kr}}(R, 0)$ were not available experimentally or theoretically. They have been modelled using a Morse-Morse-switching function-van der Waals potential,[7] with the same short range interaction as for the $\mathrm{I} \cdots \mathrm{Kr}$ pair, and a potential of the form $-\alpha_1/2R^4 - \alpha_2/2R^6$ for the long range, where α_1 and α_2 are the first and second polarizability of the Kr atom.[7,11]

Similarly to the procedure of Ref. 8, the force field of the ion-pair manifold is made polarizable with the addition of the diagonal matrix $\mathbf{W}_{\mathrm{pol}} = W_{\mathrm{pol}} \mathbf{I}_{18\times 18}$, which includes charge-induced dipole and induced dipole-induced dipole interactions. The induction energy W_{pol} is evaluated in the electrostatic approximation[12] as

$$W_{\mathrm{pol}} = -\sum_{i=1}^{N_{\mathrm{Kr}}} \boldsymbol{\mu}_i^{\mathrm{ind}} \cdot \left(\frac{\mathbf{R}_{iA}}{R_{iA}^3} - \frac{\mathbf{R}_{iB}}{R_{iB}^3} \right) - \sum_{i,j=1}^{N_{\mathrm{Kr}}} \boldsymbol{\mu}_i^{\mathrm{ind}} \mathbf{T}_{ij} \boldsymbol{\mu}_j^{\mathrm{ind}} + \sum_{i=1}^{N_{\mathrm{Kr}}} \frac{\boldsymbol{\mu}_i^{\mathrm{ind}} \cdot \boldsymbol{\mu}_j^{\mathrm{ind}}}{2\alpha_1} \ , \tag{S9}$$

Table S2 The 9×9 I–Kr interaction matrix $\mathbf{W}_{\mathrm{I^+Kr}}(R,0)$ in the interaction frame, where $|J,M\rangle$ basis refer to the $\mathrm{I^+\cdots Kr}$ connecting axis [see Eq. (S8)]

$\lvert J,M\rangle$	$\lvert 0,0\rangle$	$\lvert 1,0\rangle$	$\lvert 1,\pm1\rangle$	$\lvert 2,0\rangle$	$\lvert 2,\pm1\rangle$	$\lvert 2,\pm2\rangle$
$\lvert 0,0\rangle$	$(W_\Sigma+2W_\Pi)/3$	0	0	$\sqrt{2}(W_\Pi-W_\Sigma)/3$	0	0
$\lvert 1,0\rangle$	0	W_Π	0	0	0	0
$\lvert 1,\pm1\rangle$	0	0	$\delta_{MM'}(W_\Sigma+W_\Pi)/2$	0	$\pm\delta_{MM'}(W_\Pi-W_\Sigma)/2$	0
$\lvert 2,0\rangle$	$\sqrt{2}(W_\Pi-W_\Sigma)/3$	0	0	$(2W_\Sigma+W_\Pi)/3$	0	0
$\lvert 2,\pm1\rangle$	0	0	$\pm\delta_{MM'}(W_\Pi-W_\Sigma)/2$	0	$(W_\Sigma+W_\Pi)/2$	0
$\lvert 2,\pm2\rangle$	0	0	0	0	0	W_Π

where $\mathbf{T}_{ij}=\boldsymbol{\nabla}_i\boldsymbol{\nabla}_j(1/R_{ij})$ is the dipole-dipole tensor, and the atomic induced dipoles are obtained by solving the equations

$$\boldsymbol{\mu}_i^{\mathrm{ind}}=\alpha\left[\frac{\mathbf{R}_{iA}}{R_{iA}^3}-\frac{\mathbf{R}_{iB}}{R_{iB}^3}+\sum_{j=1}^{N_{\mathrm{Kr}}}\mathbf{T}_{ij}\boldsymbol{\mu}_j^{\mathrm{ind}}\right]. \tag{S10}$$

The complex 10×10 diabatic potential matrix for the first tier has the form of Table S3. Analogously to the covalent case, the diagonal potentials are totally symmetric functions of the coordinates, and the off-diagonal couplings transform according to the irreps of the $D_{2\mathrm{h}}$ group which result from the direct products $\Gamma(\overline{\psi}_i)\times\Gamma(\overline{\psi}_j)$.

Table S3 The form of the potential matrix $\mathbf{W}$ for the 10 ion-pair state of the first tier, as resulting from the DIM model applied to the $\mathrm{I^+I^-}$ molecule in a $D_{2\mathrm{h}}$ crystal cage. The diagonal potentials are totally symmetric (A_g) functions of the vibrational coordinates; the irrep of the off-diagonal coupling functions is indicated by the subscript

	$\lvert\overline{\psi}_1\rangle$	$\lvert\overline{\psi}_2\rangle$	$\lvert\overline{\psi}_3\rangle$	$\lvert\overline{\psi}_4\rangle$	$\lvert\overline{\psi}_5\rangle$	$\lvert\overline{\psi}_6\rangle$	$\lvert\overline{\psi}_7\rangle$	$\lvert\overline{\psi}_8\rangle$	$\lvert\overline{\psi}_9\rangle$	$\lvert\overline{\psi}_{10}\rangle$
$\lvert\overline{\psi}_1\rangle$	$W^{(1,2)}$									
$\lvert\overline{\psi}_2\rangle$	0	$W^{(1,2)}$								
$\lvert\overline{\psi}_3\rangle$	$\sqrt{3}W_{B_{2g}}$	$\mathrm{i}\sqrt{3}W_{B_{3g}}$	$W^{(3)}$							
$\lvert\overline{\psi}_4\rangle$	$\mathrm{i}\sqrt{3}W_{B_{3g}}$	$\sqrt{3}W_{B_{2g}}$	0	$W^{(4)}$						
$\lvert\overline{\psi}_5\rangle$	$W_{B_{1u}}$	$\mathrm{i}W_{A_u}$	$W_{B_{3u}}$	$\mathrm{i}W_{B_{2u}}$	$W^{(5)}$					
$\lvert\overline{\psi}_6\rangle$	W_{A_g}	$\mathrm{i}W_{B_{1g}}$	$W_{B_{2g}}$	$\mathrm{i}W_{B_{3g}}$	$W^{(4)}_{B_{1u}}$	$W^{(6)}$				
$\lvert\overline{\psi}_7\rangle$	$\mathrm{i}\sqrt{3}W_{B_{2u}}$	$\sqrt{3}W_{B_{3u}}$	$\mathrm{i}\frac{\sqrt{3}}{2}W_{A_u}$	$W'''_{B_{1u}}$	$-\mathrm{i}W_{B_{3g}}$	$-\mathrm{i}W_{B_{2u}}$	$W^{(7)}$			
$\lvert\overline{\psi}_8\rangle$	$\sqrt{3}W_{B_{3u}}$	$\mathrm{i}\sqrt{3}W_{B_{2u}}$	$W''_{B_{1u}}$	$-\mathrm{i}\frac{\sqrt{3}}{2}W_{A_u}$	$W_{B_{2g}}$	$W_{B_{3u}}$	0	$W^{(8)}$		
$\lvert\overline{\psi}_9\rangle$	$W'_{B_{1u}}$	0	$\sqrt{3}W_{B_{3u}}$	$-\mathrm{i}\sqrt{3}W_{B_{2u}}$	W_{A_g}	$W_{B_{1u}}$	$-\mathrm{i}\sqrt{3}W_{B_{3g}}$	$\sqrt{3}W_{B_{2g}}$	$W^{(9,10)}$	
$\lvert\overline{\psi}_{10}\rangle$	0	$W'_{B_{1u}}$	$-\mathrm{i}\sqrt{3}W_{B_{2u}}$	$\sqrt{3}W_{B_{3u}}$	$-\mathrm{i}W_{B_{1g}}$	$-\mathrm{i}W_{A_u}$	$\sqrt{3}W_{B_{2g}}$	$-\mathrm{i}\sqrt{3}W_{B_{3g}}$	0	$W^{(9,10)}$

2 Selection of the modes included in the quantum dynamical simulation

2.1 Totally symmetric modes

The procedure to identify the relevant totally symmetric modes is essentially identical to the one used in Ref. 13 to construct a potential energy surface for the isolated B state. In brief, the geometry of the embedded cluster is optimized for the X state, the mass-weighted Hessian matrix is calculated and diagonalised to get the squared frequencies ω_i^2 and the normal modes q_i', dimensionless normal modes are finally obtained by frequency-weighting, $q_i = q_i'\sqrt{\hbar/\omega_i}$.

The modes expected to be the most active are identified by calculating classical trajectories evolving on the four diabatic surfaces of the states from ψ_7 to ψ_{13}. For each surface, the initial positions and momenta are sampled from the Wigner distributions

$$W_0(q_i,p_i) = \frac{1}{\pi}\exp\left[-\left(q_i - q_i^{(0)}\right)^2 - p_i^2\right] \ , \tag{S11}$$

where $q_i^{(0)} = 0$ for $i \neq 1$; $q_1^{(0)}$ is set to zero for the dynamics on the B state, and in the other cases it is chosen as the crossing point with the B state curve. The modes are sorted in order of dynamical relevance by evaluating the time-averaged dimensionless phase space variances

$$\overline{\Sigma}_i = \left(\frac{1}{T}\int_0^T \left\langle q_i^2 + p_i^2\right\rangle \mathrm{d}t\right) - 1 \ , \tag{S12}$$

which is large for the modes with the largest displacements from their initial average position. The quantities $\overline{\Sigma}_i$ obtained in the classical simulations on four diabatic surfaces are shown in the bar charts of Fig. S1 for $i > 1$. The non-totally symmetric modes remain nearly undisplaced during the dynamics. Among the a_g modes, the most displaced ones in the dynamics on the B state are the Kr belt atoms stretching mode q_5 and, to a lesser extent, q_{64}, q_{111} and q_{115}. These coordinates and, additionally, the modes q_{62}, q_{164}, q_{201}, q_{210} and q_{215} are also relevant for the description of the motion on the predissociative surfaces.

2.2 Non-totally symmetric modes

As shown in Table 1 of the Appendix of the main paper, the six states from ψ_7 to ψ_{13} have all different symmetries. Therefore, the six diabatic couplings V_α between the B state and the predissociative states are mediated by modes belonging to six different irreps α (see Table 2 of the Appendix of the main paper). In the reduced dimensionality model, one effective mode q_α is constructed for each irrep as linear combination of normal modes

$$q_\alpha = N_\alpha \sum_j q_j \left(\frac{\partial V_\alpha}{\partial q_j}\right)_{q_*} \ , \ \text{with} \ N_\alpha = \left[\sum_j \left(\frac{\partial V_\alpha}{\partial q_j}\right)_{q_*}\right]^{-\frac{1}{2}} \ , \tag{S13}$$

where the derivatives $(\partial V_\alpha/\partial q_j)_{q_*}$ are evaluated at the diabatic crossing points between the potential curves of the states ψ_7 and ψ_n, with the bath modes fixed to zero (i.e. at the X state minimum).

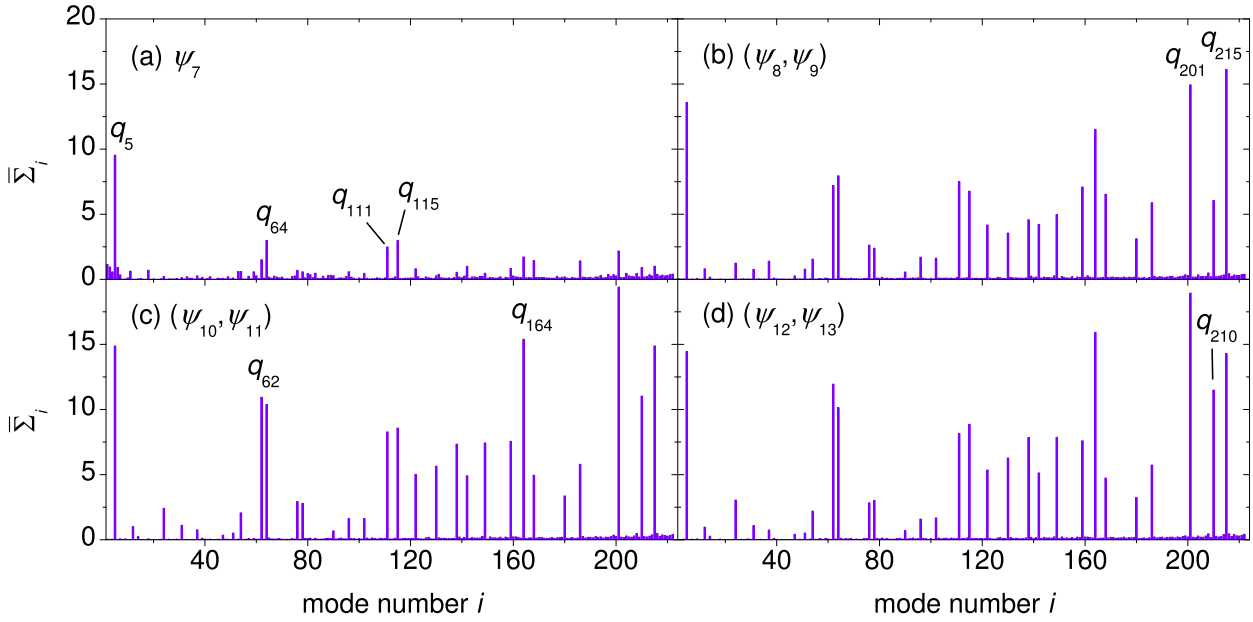

Figure S1 (a-d) Time-integrated phase space variances $\bar{\Sigma}_i$ of the normal modes of the I_2Kr_{72} cluster embedded in the Kr_{130} cage, obtained from the calculated full-dimensional classical trajectories evolving on the isolated diabatic surfaced of the states from ψ_7 to ψ_{13}. (e) The modes of the I_2Kr_{72} cluster included in the quantum dynamical simulations.

The irrep of the diabatic coupling functions V_α are such that $\alpha = \Gamma(\psi_7) \otimes \Gamma(\psi_n)$. The construction of Eq. (S13) has a rigorous foundation,[14,15] and it has been shown that even a single effective mode provides quantitative estimates of diabatic transition rates and probabilities.[16–18]

Eq. (S13), applied to the six relevant couplings, yields six non-totally symmetric effective modes which belong to different irreps. Two additional symmetry-breaking modes are constructed by applying the same equation to the potentials $V^{(2)}_{B_{1u}}$ and $V_{B_{1g}}$ (with the gradients evaluated at $q_1 = 30$), which mediate the coupling between the predissociative states and the low lying bound states, from ψ_1 to ψ_6. The mode $q^{(2)}_{B_{1u}}$ is then orthogonalized with respect to $q^{(1)}_{B_{1u}}$. The frequencies associated to the effective modes, evaluated using the formulas of Ref. 14, are given in Fig. 2 of the main paper.

3 Transition dipole moment functions

The transition dipole moment functions for the $B \longleftarrow X$, $E \longleftarrow B$ and $\beta \longleftarrow A$ excitations are adapted from the experimentally derived expressions,[19–21] and have the following form:

$$\mu_{BX}(q_1) = \frac{\exp\left[-0.00144(q_1-19.7)^2\right]}{q_1+54.1} 36.8\, ea_0 \ , \tag{S14a}$$

$$\mu_{EB}(q_1) = \frac{187.031\, ea_0}{15012.2+(q_1-25.56)^2} \ , \tag{S14b}$$

$$\mu_{\beta A}(q_1) = 0.27116 \mathrm{e}^{-0.04948 q_1}\, ea_0 \ . \tag{S14c}$$

4 Electronic dephasing

The nonadiabatic dynamics starting on the B state give rise to a superposition of high-dimensional wave packets located on different diabatic surfaces. When an observation is done on the I_2 chromophore, the Kr bath is traced out, and the precise phase relation between the wave packet on the B state and those on the predissociative surfaces tends to disappear. Such electronic dephasing si typically monitored in time by evaluating the coherences $\langle\Psi,t|\psi_7\rangle\langle\psi_j|\Psi,t\rangle$.

Since the initial wave packet on the B surface is totally symmetric, the wave packets evolving in the states ψ_j have a symmetry $\Gamma_7\times\Gamma_j\neq A_g$, where Γ_j is the irrep of the state ψ_j. Therefore, the coherences vanish upon integration of the vibrational coordinates. However, the reason for the formally vanishing coherence is purely topological, i.e. it is related to the geometric phase effect, and has nothing to do with the environment-driven decoherence.

In order to obtain an estimate for the electronic dephasing time, due to the interaction with the bath, the quantities

$$\varsigma_j(q_1,t)=\left\langle\Psi,t|\psi_7\rangle q_\Gamma\langle\psi_j|\Psi,t\right\rangle_{\mathbf{q}_{\text{bath}}} \tag{S15}$$

are evaluated. In Eq. (S15) the integration is performed only over the bath modes, and q_Γ is the symmetry-breaking mode which belongs to the appropriate irrep, $\Gamma(\psi_7)\times\Gamma(\psi_j)$, in order that the integral does not vanish (in principle, any odd function of q_Γ could be used).

The quantities ς_j are plotted in Fig. S2 for the eight predissociative states, for the dynamics initiated by impulsive $B\longleftarrow X$ excitation. The "coherences" between the B state and the crossing states from ψ_8 to ψ_{13} are visible only in certain time windows, which roughly correspond to the times at which the internal conversion events of Fig. 3(a) of the main paper take place. The wave packets formed in different diabatic states dephase so rapidly that the time windows for the vibronic coherences last for only half-vibrational period (150–200 fs). The coherences between the B state and the states ψ_4 and ψ_5 are formed transiently around 900 fs and have a similar duration.

Similar to the excitonic transport in multichromophoric systems, long-lived coherences are often associated with parallel wave packet evolution across several coupled electronic states.[22,23] That is, rapid population exchange between the electronic states does not preclude concerted wave packet motion. In the present case, the population dynamics lasts for 1.5 ps, which is indeed the time scale for which most of the coherences of Fig. S2 are observed. Note however that the coherences ς_{12} and ς_5 emerge also around 2200 fs, i.e. much after the time needed for the equilibration of the electronic populations.

References

[1] R. M. Bowman, M. Dantus and A. H. Zewail, *Chem. Phys. Lett.*, 1989, **161**, 297.

[2] N. F. Scherer, D. M. Jonas and G. R. Fleming, *J. Chem. Phys.*, 1993, **99**, 153.

[3] C. Teichteil and M. Pelissier, *Chem. Phys.*, 1994, **180**, 1.

[4] T. Kiljunen, M. Bargheer, M. Gühr and B. Schmidt, *Phys. Chem. Chem. Phys.*, 2004, **6**, 2185.

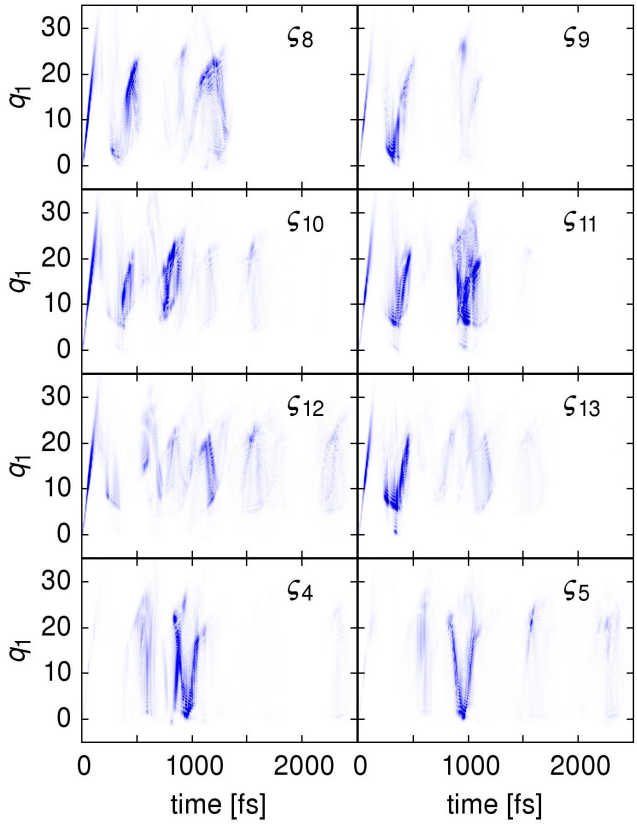

Figure S2 Electronic dephasing of I_2 in crystal Kr. Absolute value of the vibronic coherences $|\varsigma_j(q_1,t)|$ between the B state and the predissociative states ψ_j.

[5] C. H. Becker, P. Casavecchia and Y. T. Lee, *J. Chem. Phys.*, 1979, **70**, 2986.

[6] V. Aquilanti, E. Luzzatti, F. Pirani and G. G. Volpi, *J. Chem. Phys.*, 1988, **89**, 6165.

[7] Y. Zhao, I. Yourshaw, G. Reiser, C. C. Arnold and D. M. Neumark, *J. Chem. Phys.*, 1994, **101**, 6538.

[8] V. S. Batista and D. F. Coker, *J. Chem. Phys.*, 1997, **106**, 6923.

[9] K. S. Viswanathan and J. Tellinghuisen, *J. Mol. Spectrosc.*, 1983, **101**, 285.

[10] V. Aquilanti, R. Candori and F. Pirani, *J. Chem. Phys.*, 1988, **89**, 6157.

[11] C. Hättig and B. A. Hess, *J. Phys. Chem.*, 1996, **100**, 6243.

[12] E. L. Pollock and B. J. Alder, *Phys. Rev. Lett.*, 1978, **41**, 903.

[13] D. Picconi, J. A. Cina and I. Burghardt, *J. Chem. Phys.*, 2019, **150**, 064111.

[14] L. S. Cederbaum, E. Gindensperger and I. Burghardt, *Phys. Rev. Lett.*, 2005, **94**, 113003.

[15] E. Gindensperger, I. Burghardt and L. S. Cederbaum, *J. Chem. Phys.*, 2006, **124**, 144103.

[16] H. Tamura, J. G. S. Ramon, E. R. Bittner and I. Burghardt, *Phys. Rev. Lett.*, 2008, **100**, 107402.

[17] R. Martinazzo, K. H. Hughes, F. Martelli and I. Burghardt, *Chem. Phys.*, 2010, **377**, 21.

[18] D. Picconi, A. Lami and F. Santoro, *J. Chem. Phys.*, 2012, **136**, 244104.

[19] J. Tellinghuisen, *J. Chem. Phys.*, 2011, **134**, 084301.

[20] J. Tellinghuisen, *Phys. Rev. Lett.*, 1975, **34**, 1137.

[21] J. Tellinghuisen, *Chem. Phys. Lett.*, 1974, **29**, 359.

[22] A. D. Sio, F. Troiani, M. Maiuri, J. Réhault, E. Sommer, J. Lim, S. F. Huelga, M. B. Plenio, C. A. Rozzi, G. Cerullo, E. Molinari and C. Lienau, *Nat. Comm.*, 2016, **7**, 13742.

[23] W. Popp, M. Polkehn, R. Binder and I. Burghardt, *J. Phys. Chem. Lett.*, 2019, **10**, 3326.